

Mathematical and In Silico Analysis of Synthetic Inhibitory Circuits That Program Self-Organizing Multicellular Structures

Published as part of ACS Synthetic Biology virtual special issue "Mammalian Cell Synthetic Biology".

Calvin Lam*



Cite This: *ACS Synth. Biol.* 2024, 13, 1925–1940



Read Online

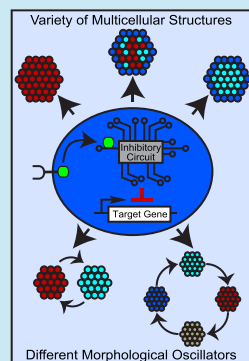
ACCESS |

Metrics & More

Article Recommendations

Supporting Information

ABSTRACT: Bottom-up approaches are becoming increasingly popular for studying multicellular self-organization and development. In contrast to the classic top-down approach, where parts of the organization/developmental process are broken to understand the process, the goal is to build the process to understand it. For example, synthetic circuits have been built to understand how cell–cell communication and differential adhesion can drive multicellular development. The majority of current bottom-up efforts focus on using activatory circuits to engineer and understand development, but efforts with inhibitory circuits have been minimal. Yet, inhibitory circuits are ubiquitous and vital to native developmental processes. Thus, inhibitory circuits are a crucial yet poorly studied facet of bottom-up multicellular development. To demonstrate the potential of inhibitory circuits for building and developing multicellular structures, several synthetic inhibitory circuits that combine engineered cell–cell communication and differential adhesion were designed, and then examined for synthetic development capability using a previously validated in silico framework. These designed inhibitory circuits can build a variety of patterned, self-organized structures and even morphological oscillations. These results support that inhibitory circuits can be powerful tools for building, studying, and understanding developmental processes.



KEYWORDS: synthetic biology, computational biology, synthetic development, synthetic receptors, amplifiers, tissue engineering, self-organization, morphogenesis

INTRODUCTION

The development of multicellular organisms is an intricate, highly coordinated dance that has fascinated scientists for centuries.^{1–9} With minimal external control, individual units communicate with one another, alter their behavior accordingly, and self-organize into ornately patterned, functional structures.^{10–17} Understanding these developmental processes is a longstanding goal of biology; it not only provides insight into multicellular life but also insight for clinical applications, such as tissue engineering and regenerative medicine.^{10,11,13–28}

However, understanding these multicellular developmental processes is notoriously difficult. The classic top-down “break-it-to-understand-it” approach focuses on breaking a part of the process to understand the process, but breaking a part can affect the subsequent and parallel parts.^{15,16,29} This approach informs of the necessity of the part but not necessarily the function(s) of the part.¹⁶

In recent years, a complementary strategy has emerged through the field of synthetic biology. The field’s modular tools allow programming and controlling cells, enabling a bottom-up “build-it-to-understand-it” approach. In contrast to the top-down approach, the bottom-up approach seeks to join together parts that can construct/build the process, thereby providing understanding of the process.^{10,11,13,14,16–23,25–27,29,30} Though

nascent, this approach has proven powerful thus far.^{10,31} Using synthetic juxtarcline receptors as parts to control cell–cell signaling processes, Morsut et al. demonstrated that such processes can build complex multicellular multilayered patterns.³¹ Adding differential adhesion as a part illustrated that processes combining juxtarcline signaling with differential adhesion can build a variety of 3D multicellular patterned structures.¹⁰ These constructed processes provide insight into how basic components such as cell signaling and adhesion expression can direct complex self-organization. Moreover, these synthetic processes have features such as regeneration, cell fate divergence, and symmetry breaking, providing insight into how these features occur in native multicellular developmental processes.^{10,31}

The majority of these bottom-up, synthetic development efforts emphasize activation. For instance, the above studies used a synthetic juxtarcline receptor to activate expression of a

Received: April 1, 2024

Revised: May 5, 2024

Accepted: May 7, 2024

Published: May 23, 2024



target gene (Figure 1A).^{10,31} With different fluorescent reporter and adhesion cadherin genes as the target gene, these activatory

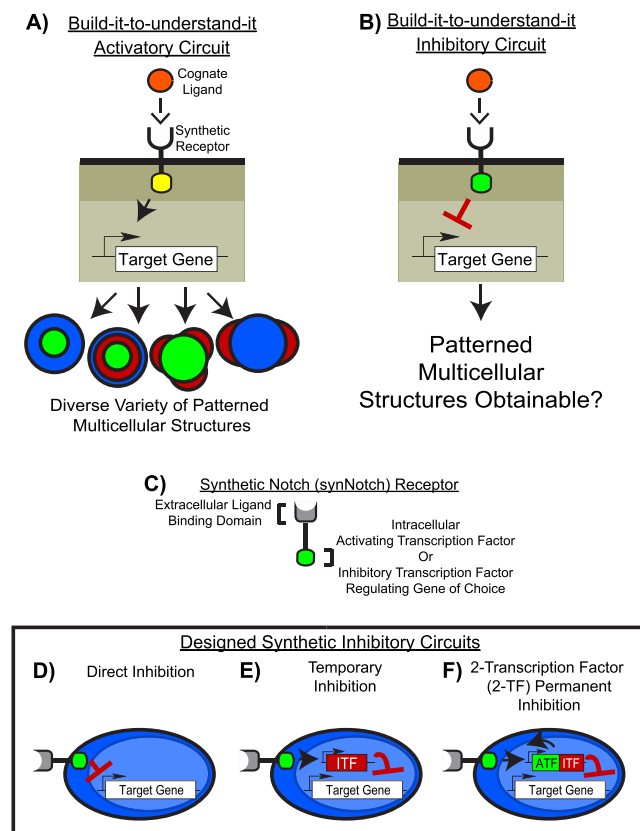


Figure 1. Design of the synthetic inhibitory circuits for bottom-up multicellular development. (A) Majority of bottom-up “build-it-to-understand-it” approaches for multicellular development use activatory circuits. A target gene is activated to drive development. Such circuits are capable of building multitudes of structures. (B) Inhibitory circuits, in contrast, are rarely used in the bottom-up approach. Are they also capable of building various multicellular structures? (C) Synthetic Notch (synNotch) receptor is a synthetic receptor modular in both ligand binding and intracellular domain. Ligand binding domain allows sensing a ligand of choice and intracellular domain allows releasing an activating or inhibitory transcription factor of choice. (D) Direct inhibition circuit has the synNotch receptor release an inhibitory transcription factor to directly repress target gene expression.³¹ (E) Temporary inhibition circuit has the synNotch receptor first drive an inhibitory transcription factor (ITF) that then represses target gene expression. This circuit should result in temporarily prolonging gene repression. (F) 2-TF permanent inhibition circuit has the synNotch receptor drive a transgene cassette with an activating transcription factor (ATF) and ITF. ATF drives itself and the ITF, permanently expressing ITF to permanently repress gene expression.

circuits, when programmed into cells, yield developmental processes that can build a variety of patterned, multicellular self-organizing structures (Figure 1A).^{10,31}

To date, inhibitory circuits, despite being integral to native multicellular developmental processes, have been much less used in synthetic development (Figure 1B). Nonetheless, the few current results support that inhibitory circuits could be a powerful strategy for building and understanding multicellular development. For instance, using inhibitory circuits to build morphogen gradients revealed that double negative signaling logic coupled with negative feedback improves gradient pattern formation in the Sonic Hedgehog pathway.¹⁴ Using inhibitory

circuits to inhibit morphogen activity allows the formation of sharp gradient boundaries.¹¹ Inhibitory circuits coupled with differential adhesion can drive the formation of at least one type of patterned 3D structure.¹⁰

To investigate the potential of inhibitory circuits for bottom-up multicellular development, several generalizable synthetic inhibitory circuits were designed in this study. These circuits are driven by the synthetic Notch (synNotch) receptor, a powerful, fully modular receptor that is capable of both activating and inhibiting gene expression.^{31,32} Upon binding the juxtarcline cognate ligand, this receptor releases a transcription factor (TF) controlling the gene of choice (Figure 1C).^{31,32} For gene activation, an activating transcription factor (ATF) is released to drive target gene expression. For gene inhibition, the receptor can either directly repress gene expression by releasing an inhibitory transcription factor (ITF)³¹ or indirectly by driving expression of an ITF that then represses target gene expression.¹⁰ The flexibility of the synNotch receptor allows designing inhibitory circuits with varying signaling and temporal dynamics for building and developing multicellular structures (Figure 1D–F).¹⁸ The published accompanying study shows how activatory circuits with varying spatiotemporal control can be used for bottom-up multicellular development.¹⁸

Moreover, the use of the synNotch receptor allows employing a previously validated computational strategy, enabling a thorough exploration of the developmental capabilities of these inhibitory circuits.^{18,19} The Generalized Juxtarcline Signaling Model (GJSM) set of equations allows simple and intuitive modeling of synNotch circuits. SynNotch circuits are first converted to GJSM equations and then implemented into in silico cells (via a framework such as the cellular Potts model^{33–35}). This computational approach can successfully predict the developmental structures that result from programming in vitro cells with synNotch circuits.^{19,36} This computational approach is ideal for exploring these circuits’ capabilities for bottom-up multicellular development; it allows a rapid and systematic investigation into circuit behavior across different parameters.¹⁸

Here, I show that the designed inhibitory circuits are capable of their intended behavior. When the computational approach is benchmarked against native and synthetic systems, it successfully recapitulates features of these systems. When the designed circuits are combined with differential adhesion and implemented into in silico cells, the model predicts that these inhibitory circuits can give rise to a variety of patterned multicellular structures. Of the structures obtained, the model predicts the only known in vitro patterned structure (expected as this was demonstrated in the original study¹⁹), but the model also predicts that this only known structure is but a fraction of the morphologies possible. Further examination of the various structures indicated that one circuit is capable of morphological oscillations, but these oscillations dampen quickly, suggesting that further temporal regulation is required. Incorporating activating transcriptional amplifiers to additionally modulate temporal control revealed that the amplifiers can not only improve but even rescue oscillations. These results support that inhibitory circuits can be powerful tools for bottom-up synthetic development.

RESULTS

Design of the Synthetic Inhibitory Circuits. The direct inhibition circuit is the simplest of the designed inhibitory circuits. It uses a synNotch receptor that, upon binding its

juxtarine cognate ligand, releases a transcriptional repressor inhibiting expression of the target gene (Figure 1D).³¹ Because repression is directly mediated by the synNotch receptor, this circuit is highly dependent on the presence of the cognate ligand to maintain gene repression; loss of the signaling ligand should quickly result in decrease of gene repression.^{18,31,32} Thus, this design offers basic spatial control with minimal temporal control.^{31,32}

To demonstrate how inhibitory circuits can be used for bottom-up multicellular development, it would be ideal to also test other inhibitory circuits with additional levels of temporal control. Thus, two additional circuits were designed: the temporary inhibition circuit and 2-transcription factor (2-TF) permanent inhibition circuit.

In the temporary inhibition circuit, the synNotch receptor's modularity to also activate gene expression is employed.^{10,31,32} The synNotch receptor drives expression of an ITF that then inhibits target gene expression (Figure 1E).¹⁰ Repression is now dependent on the ITF level, rather than the synNotch signal, and thus gene repression should continue even when synNotch signaling is lost, as long as the ITF remains elevated enough to continue repression. Compared to the direct inhibition circuit, this circuit should enable temporarily prolonging gene repression.

In the 2-TF permanent inhibition circuit, the synNotch receptor activates expression of both an ATF and an ITF (Figure 1F). An example gene cassette would be the ATF and ITF genes linked by an internal ribosomal entry site or ribosomal skipping site, and expression controlled by a promoter activated by the synNotch receptor. The ATF drives itself and the ITF, providing a positive feedback loop for permanent ITF expression and thus should result in permanent gene repression.^{18,37–39}

Circuits Inhibit Gene Expression with Temporal Control over Repression as Designed. With the circuits designed, they were converted into GJSM equations and implemented into *in silico* cells using the CompuCell3D cellular Potts framework.^{33,34} This combination was previously tested for modeling synNotch circuits for bottom-up multicellular development.^{18,19,36} See prior works^{18,19,36} and the Methods section for more details. These circuits were then tested for their temporal control over gene repression. Blue cells, blue as they constitutively express blue reporter, were programmed to express a synNotch receptor that responds to the orange ligand on orange cells (Figure 2A). In the direct inhibition circuit, the synNotch receptor directly inhibits blue reporter expression (Figure 2A). In the temporary inhibition circuit, the synNotch receptor drives an ITF that then inhibits blue reporter expression (Figure 2A). In the 2-TF permanent inhibition circuit, the synNotch receptor drives both an ATF and ITF. The ATF acts as a permanent amplifier of ITF expression and ITF inhibits blue reporter expression (Figure 2A). These cells were then tested for their temporal control over gene repression using a simple cell-cell signaling setup from the accompanying study that examines activatory circuits.¹⁸

A blue cell, imbued with one of the inhibitory circuits, is seeded with 3 orange sender cells. Cells are cubic and frozen (i.e., locked in shape, volume, and surface area) to maintain consistent synNotch signaling (Figure 2B). At 25,000 timesteps, orange senders are deleted to test how ligand and synNotch signaling loss affects repression (Figure 2B). This setup allows controlling the exact level of synNotch signaling at a given time, thus enabling simultaneous testing of the circuit's ability to inhibit reporter expression and temporality of repression.¹⁸

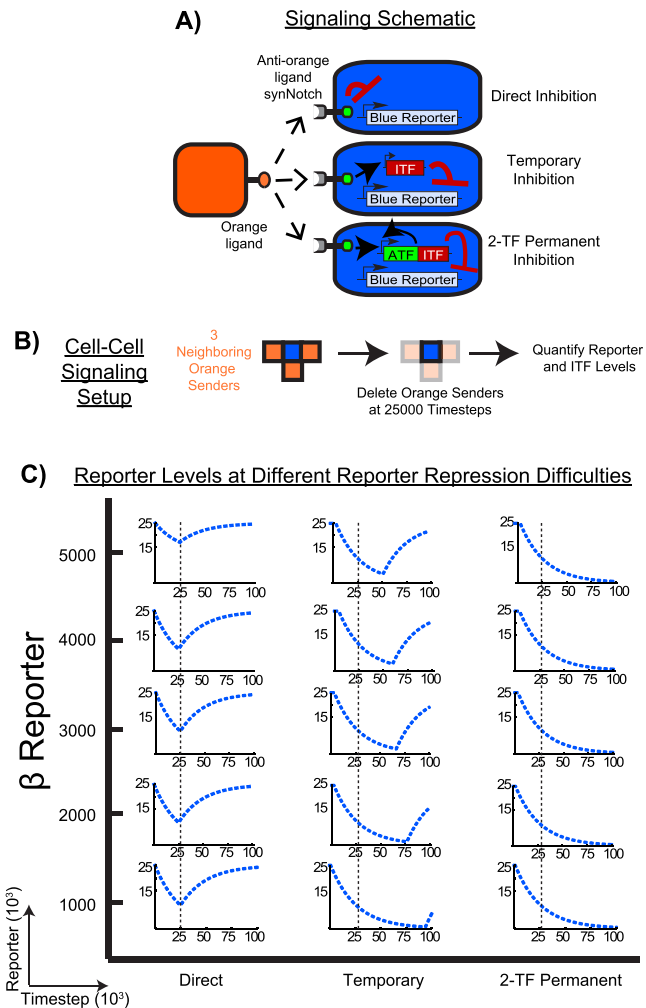


Figure 2. Inhibitory circuits inhibit gene expression as designed. (A) Signaling schematic for testing if the inhibitory circuits operate as designed. Blue cells are programmed with an anti-orange ligand synNotch that triggers one of the inhibitory circuits to repress blue reporter expression. (B) Cell-cell signaling test setup, where a blue cell is seeded with 3 orange neighbor cells and orange cells are deleted at 25,000 timesteps to determine how orange ligand-synNotch signaling loss affects blue reporter repression. (C) Blue reporter traces from the signaling test setup at different blue reporter repression difficulties (β reporter). Cells with the direct inhibition circuit lost gene repression immediately after orange neighbor loss, consistent with the circuit's minimal temporal control design. These results are consistent with *in vitro* direct synNotch signaling dynamics.^{18,31,32} In contrast, the temporary inhibition circuit maintained repression for some time despite synNotch signaling loss. The 2-TF permanent inhibition circuit maintained permanent blue reporter repression even after signaling loss. These results confirm that the circuits operate as designed. See Figure S1 for blue reporter repression difficulties where the circuits begin to fail. One trace shown per condition. Simulations run for 100,000 timesteps.

In GJSM equations for synNotch circuits, gene expression and repression are modeled by several parameters. For gene activation or gene expression, β models gene expression difficulty while for inhibition or gene repression, β models gene repression difficulty. Higher values of β model higher expression/repression difficulties while lower values model lower expression/repression difficulties. Lower β values, however, do increase the risk of background gene expression/repression.^{18,19,36} κ models protein product degradation rate/

saturation levels. See the accompanying study,¹⁸ the original study¹⁹ or the *Methods* section for further details.

Thus, the circuits were first checked for background gene inhibition. At reporter repression difficulties (β reporter) ≥ 1000 , there was no background repression in all designed circuits (Figure S1A). The circuits were then tested at higher repression difficulties and all circuits were able to yield reporter repression (Figure 2C).

The direct inhibition circuit was able to inhibit reporter expression up to β reporter = 5000 (Figure 2C and Figure S1B) and as predicted, had high spatial but minimal temporal control. Loss of synNotch signaling via loss of orange neighbors at 25,000 timesteps resulted in immediate loss of blue reporter repression (Figure 2C). This temporal dynamic is consistent with reported synNotch signaling dynamics in vitro.^{18,31,32}

In contrast, the temporary inhibition circuit repressed reporter expression up to β reporter = 12,000 and maintained inhibition for some time even after loss of orange neighbors (Figure 2C and Figure S1B). Reporter levels eventually increased once again due to the ITF's reliance on synNotch signaling to remain elevated (Figure 2C and Figure S1B), confirming the temporary inhibition design. Compared to the direct inhibition circuit, there was a time delay to repression due to incorporating an additional ITF step, representing biological processes, such as ITF translation and maturation (Figure S1C).^{18,19}

The 2-TF permanent inhibition circuit repressed reporter expression up to β reporter = 18,000 and maintained permanent blue reporter repression even after loss of the orange neighbors (Figure 2C and Figure S1B). This is due to the ATF's positive feedback loop allowing permanent ITF expression and thus permanent reporter repression, confirming the permanent inhibition design. Like the temporary inhibition circuit, there was also a time delay to repression due to the ITF step (Figure S1C). The delay is identical to that of the temporary inhibition circuit as synNotch signaling in this setup was strong enough to drive ITF expression. It was only after the loss of SNs did the ATF contribute to maintaining ITF expression (Figure S1C).

Similar results were obtained with 1 and 6 orange sender neighbors (data not shown). While all the inhibition circuits operate as designed, it is important to note that they fail at some parameter sets (Figure S1B). Thus, circuit behavior is not solely defined by circuit design, but by its parameters as well.¹⁸

Inhibitory Circuits Recapitulate Patterning of Native and Synthetic Processes. With data supporting that the inhibitory circuits function as designed, the model was then benchmarked against known inhibitory processes to test its recapitulative capability as in the original study.¹⁹ The circuits were first benchmarked against lateral inhibition-driven patterning.^{4,40}

In lateral inhibition, cells signal to one another via the Notch receptor and the Delta ligand, with this juxtracrine signaling resulting in downregulation of Delta. In a population of cells with both Notch and Delta expression, this mechanism can drive bifurcation, forcing cells into either a Delta low or Delta high fate. In native developmental processes, this signaling can pattern a relatively uniform cell population into a "salt-and-pepper" pattern with Delta high cells surrounded by Delta low cells.^{4,40–45}

The exact lateral inhibition circuit in native processes remains unknown, but it is commonly modeled using an inhibitory circuit, typically with Notch, in response to Delta, driving expression of a repressor that then inhibits Delta expression.

This circuit can generate the "salt-and-pepper" pattern as is observed natively.^{2–4,46}

The temporary inhibition circuit is the generalized version of this circuit; the synNotch receptor, in response to blue ligands on neighboring cells, drives an ITF that then inhibits blue ligand expression (Figure 3A). A monolayer of blue cells, when programmed with the temporary inhibition circuit, bifurcates cells into either the blue ligand low (red cell) or blue ligand high (blue cell) fate (Figure 3B left). This circuit generates a "salt-and-pepper" pattern like those in a native lateral inhibition process such as chicken hair development (Figure 3B right).^{4,40} Ligand high (LH) cells are surrounded by ligand low (LL) cells similar to how hair cell antigen (HCA) high cells are surrounded by HCA low cells (Figure 3B).^{4,40} Additional "salt-and-pepper" patterns to compare between the model and *in vivo* are given in Figure S2A.

Another feature of native "salt-and-pepper" patterning is size bias; smaller cells are more likely to become Delta high while larger cells are more likely to become Delta low.^{4,40} To determine if this was also observed with the temporary inhibition circuit in silico, the average cell size of blue LH cells was compared to the average cell size of blue ligand low cells. LH cells were significantly smaller than LL cells as is observed *in vivo* (Figure S2B). The full gallery of patterns generated by the temporary inhibition circuit, organized by the parameters that generated them and colored by ligand levels to compare to *in vivo* images, is given in Figure S3. Size distribution of LH and LL cells is given as well. The full gallery of patterns generated by the temporary inhibition circuit, organized by the parameters that generated them but colored by both ligand and ITF levels, is given in Figure S4.

"Salt-and-pepper" patterning, along with size bias between LH and LL cells, was also observed with the direct inhibition circuit (Figure S5) and 2-TF permanent inhibition circuit (Figure S6). While these circuits are not the common model for lateral inhibition, these results suggest that they could still be mechanisms for "salt-and-pepper" patterning in development. Altogether, these results support that the computational approach deployed can recapitulate patterning and features of native inhibitory processes.

To further benchmark the computational model, the model was then tested against an *in vitro* synthetic lateral inhibition system,⁴¹ where several lateral inhibition circuits were designed. The first circuit used the Notch receptor to drive tTs repressor that then inhibits Delta expression, but this circuit had poor repression, failing to generate bifurcation and the "salt-and-pepper" pattern (Figure 3C top left). In the computational approach, this result is similar to that of the temporary inhibition circuit with poor repression, which can be modeled with a high β ITF value. Like the *in vitro* circuit, this high β ITF "poor repression" in silico circuit failed to generate bifurcation and the "salt-and-pepper" pattern (Figure 3C bottom left). The authors of the *in vitro* circuit remedied this by modifying their circuit to increase basal Notch level, activity via glycosylation alteration, and repressor induction, overall enhancing repression. This "enhanced repression" circuit successfully bifurcated cells to generate the target "salt-and-pepper" pattern (Figure 3C top right). While the approach cannot mechanistically model the increased Notch activity glycosylation modification, the approach should at least yield the same pattern if overall repression is enhanced (i.e., through lowering β ITF). Indeed, lowering β ITF in the temporary inhibition circuit allowed "salt-and-pepper" pattern formation as is observed *in vitro* (Figure 3C bottom right).

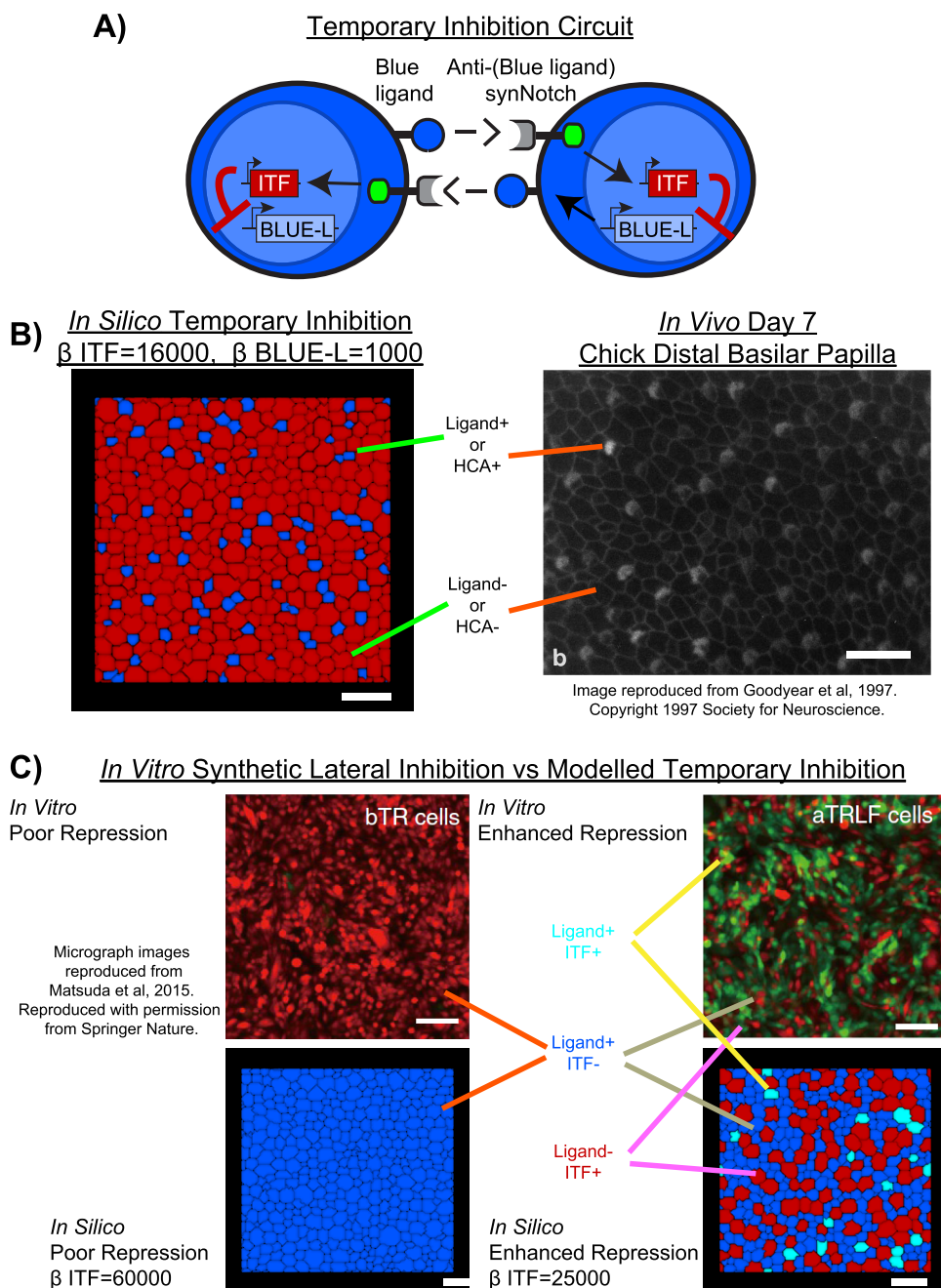


Figure 3. Inhibitory circuits can recapitulate patterning from native and synthetic inhibitory processes. (A) Temporary inhibition circuit is the generalized version of a common circuit used for studying lateral inhibition, where Notch-Delta signaling drives a repressor that inhibits Delta expression to bifurcate a uniform population of cells into Delta high and Delta low cells. The temporary inhibition circuit analogously uses synNotch-blue ligand signaling and ITF that inhibits blue ligand expression. (B) Temporary inhibition circuit can recapitulate lateral inhibition mediated chicken hair cell patterning. Blue ligand⁺/hair cell antigen (HCA)⁺ cells are surrounded by blue ligand⁻/hair cell antigen (HCA)⁻ cells. *In silico*: blue cells are blue ligand⁺, red cells are blue ligand⁻. *In vivo*: bright cells are HCA⁺, dull cells are HCA⁻, membrane staining via anti-cingulin antibody. Scalebar is 10 μ m. Image reproduced from ref 40. Copyright 1997 Society for Neuroscience. (C) Temporary inhibition circuit can recapitulate synthetic lateral inhibition as well. A poor repression circuit fails to bifurcate cells and patterns as is observed *in vitro* and *in silico*. Reengineering the circuits with improved repression should enable bifurcation and patterning, which is observed *in vitro* and *in silico*. *In silico*: blue cells are blue ligand⁺ ITF⁻, red cells are blue ligand⁻ ITF⁺, cyan cells are blue ligand⁺ ITF⁺. *In vitro*: red cells are ligand⁺ ITF⁻, green cells ligand⁻ ITF⁺, yellow cells are ligand⁺ ITF⁺. Scalebar is 100 μ m. Images reproduced from ref 41. Copyright 2015 Springer Nature. These results indicate that the computational approach can recapitulate features of both native and synthetic inhibitory systems. A representative image is given *in silico*. Additional images from the temporary inhibition circuit and other inhibitory circuits, along with their parameters, can be found in Figures S2–7. N = 3 for each *in silico* image. Simulations run for 50,000 timesteps.

bottom right). The approach, while unable to mechanistically model all biological modifications, can still recapitulate patterning as a result of poor and good repression. Overall,

these results support that the computational approach can recapitulate patterning from synthetic inhibitory processes.¹⁹

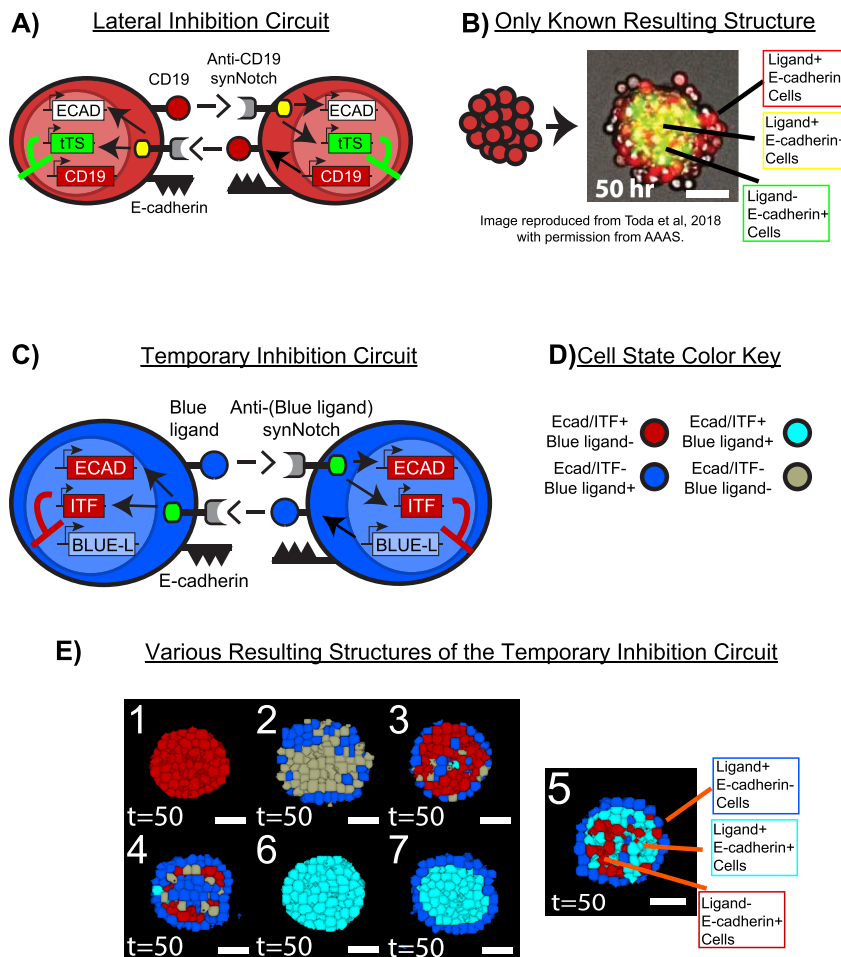


Figure 4. Temporary inhibition circuit can build a variety of multicellular structures. A) Another version of the lateral inhibition circuit,¹⁰ and thus also the temporary inhibition circuit. In this version, anti-CD19 synNotch drives E-cadherin (ECAD) and tet transcriptional repressor (tTS) that represses CD19 expression. (B) Mixing ~100 cells programmed with this circuit results in a 2-layered structure with CD19⁻ E-cadherin⁺ green cells and CD19⁺ E-cadherin⁺ yellow cells in the center with CD19⁺ E-cadherin⁻ red cells on the periphery. Micrograph reproduced from Toda et al., 2018¹⁰ with permission from AAAS. (C) Temporary inhibition circuit is the generalized version of the lateral inhibition circuit. ECAD is E-cadherin. ITF is generic representation for tTs. BLUE-L (blue ligand) is generic representation for CD19. (D) Cell state color key is given to match expression state to cell color in the subsequent images. (E) Mixing 93 blue cells programmed with the temporary inhibition circuit results in multitudes of patterned structures. A representative set of structures is given, showcasing the variety of patterned structures that can form from the temporary inhibition circuit. Each structure resulted from a different parameter set of expression difficulties for ITF/ECAD and repression difficulties for blue ligand. The full gallery of structures, along with the parameters that generated them, is given in Figure S8A. As expected, and previously shown, the model predicts the known in vitro structure.¹⁹ These results indicate that the only known structure to date is a small subset of structures possible with this circuit. $N = 3$ for each structure. Simulations run for 50,000 timesteps.

Additional images recapitulating the shift from failed patterning to successful “salt-and-pepper” patterning by decreasing repression difficulty are highlighted in a green box in Figure S7. Size bias was again noted in silico, and while not examined in the in vitro study,⁴¹ raises the possibility that size bias is also a feature of the synthetic lateral inhibition system.

Temporary Inhibition Circuit Can Build a Variety of Patterned Multicellular Structures. With the model shown capable of recapitulating patterns from both native and synthetic inhibitory processes, the circuits were then tested for their ability to build and develop multicellular structures. Another version of the lateral inhibition circuit, and thus also the temporary inhibition circuit, has been shown capable of driving 3D bottom-up synthetic development in vitro.¹⁰ In this circuit, cells signal to one another via a CD19 synNotch interaction to drive expression of the transcriptional repressor tTs and the adhesion protein E-cadherin (gene is ECAD) (Figure 4A). tTs repressor then inhibits the expression of the CD19 ligand. L929 mouse

fibroblasts programmed with this circuit reliably form only one type of patterned structure, a 2-layered structure with CD19⁻ E-cadherin⁺ green cells and CD19⁺ E-cadherin⁺ yellow cells in the center (Figure 4B). CD19⁺ E-cadherin⁻ red cells form the peripheral ring (Figure 4B).

The robust formation of the 2-layered structure is likely due to the lateral inhibition circuit being partially calibrated,¹⁰ thereby limiting the structures buildable. However, systematically investigating the generalized version of the lateral inhibition circuit, the temporary inhibition circuit (Figure 4C), revealed that this circuit design can form a wealth of patterned structures (Figure 4E and Figure S8A). The circuit was implemented in L929 (ISL929) cells^{18,19} to parallel the in vitro implementation. I tested a wide range of expression difficulties for ITF/ECAD (ITF is generic representation of tTS, gene representation is ITF) and repression difficulties for blue ligand (blue ligand is generic representation of CD19, gene is BLUE-

L). A cell color guide is given in Figure 4D. Scanned parameters are in Figure S8A.

Several structure types were formed, ranging from types 1 and 6 of highly homogeneous E-cadherin⁺ spheroids to 3, 4, 5, and 7 for 2-layered structures to 2 for mixed E-cadherin⁻ spheroids (Figure 4E). Representative structure types are shown and additional structures, organized by the parameters that generated them, are given in Figure S8A. Out of all the structure types obtained, only one (type 5 of Figure 4E), was the 2-layered structure built by the lateral inhibition circuit (Figure 4B). These results indicate that the temporary inhibition circuit can build a variety of patterned, multicellular structures. The only known *in vitro* example is but a fraction of the structures possible.

As an additional validation check, the nonadhesive version of the circuit for the 2-layered structure (Figure 4E, structure 5) was tested for its capability to recapitulate the nonadhesive structure in *vitro* (Figure S8B). Without the adhesion protein E-cadherin, cells bifurcated and formed a disorganized spheroid as is observed experimentally (Figure S8B).¹⁰

Direct Inhibition Circuit and 2-TF Permanent Inhibition Circuit Can Also Build a Variety of Patterned Multicellular Structures. Testing the direct inhibition circuit and 2-TF permanent inhibition circuit revealed that both circuits can also generate a variety of patterned structures. The direct inhibition circuit built structure types ranging from types 1 and 3 of heterogeneous E-cadherin⁺ spheroids to 4, 6, and 7 for 2-layered structures to 2 and 5 for E-cadherin⁻ spheroids (Figure 5A). The full gallery of structures, organized by the parameters that generated them, is given in Figure S9A.

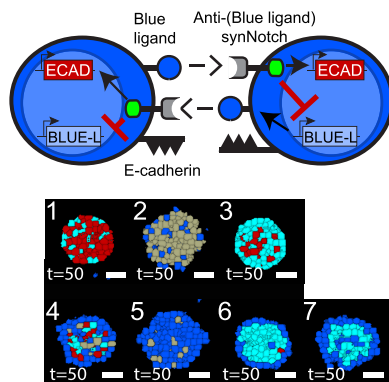
Likewise, the 2-TF permanent inhibition circuit also proved capable of building various patterned structures. Structure types ranged from 1 and 4 for highly homogeneous E-cadherin⁺ spheroids to 2, 3, and 5 for 2-layered structures (Figure 5B). Interestingly, this circuit yields less structure types compared to the other two, possibly due to its permanency in gene repression. The full gallery of structures, organized by the parameters that generated them, is given in Figure S9B.

Altogether, these results (Figures 4 and 5, Figures S8–9) demonstrate that inhibitory circuits can be powerful tools for building multicellular structures.

Temporary Inhibition Circuit Can Build Oscillatory Structures. Of the diverse structures built by the inhibitory circuits, the homogeneous spheroids of the temporary inhibition circuit (structures of types 1 and 6 of Figure 4E) were of notable interest. During the development of these structures, cells were highly uniform in the expression state of ITF/E-cadherin and blue ligand (i.e., all cells were ITF/E-cadherin⁺ blue ligand⁺ or ITF/E-cadherin⁺ blue ligand⁻, etc., see Figure 4D for all possible expression states and cell color for each state). Cells then synchronously transitioned from one expression state to another expression state (i.e., cells transitioned from one color to another color at a similar time). An example development with these features is shown in Figure 6A. These features are strikingly similar to those observed with oscillations in development.^{6,35,47,48} Because temporary gene repression is known to drive oscillation,^{6,35,47–51} these results suggest that the temporary inhibition circuit can build morphological oscillators (Figure 6B).

Extending the simulation time to 100,000 timesteps for the green outlined structures of Figure S8A revealed that the temporary inhibition circuit can indeed build morphological oscillators (Figure 6C,D, Figure S10). An initial structure of blue cells sharply transitions to cyan before transitioning to red and

A) Direct Inhibition Circuit and Various Resulting Structures



B) 2-TF Permanent Inhibition Circuit and Various Resulting Structures

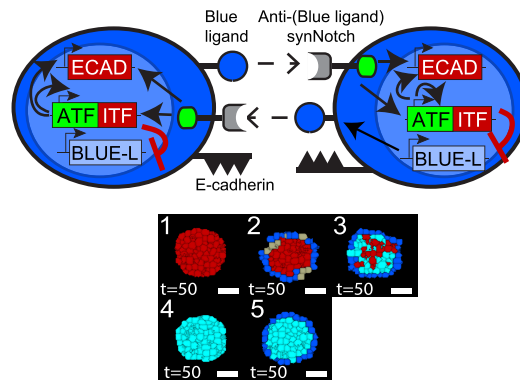


Figure 5. Designed inhibitory circuits can build multitudes of multicellular structures. (A) Direct inhibition circuit can also build various patterned structures. 93 blue cells with this circuit results in 7 different types of patterned structures. One representative structure for each pattern type is shown. Full gallery of structures is given in Figure S9A. (B) 2-TF permanent inhibition circuit can also build various patterned structures. 93 blue cells with this circuit results in 5 different types of patterned structures. One representative structure for each pattern type is shown. Full gallery of structures is given in Figure S9B. $N = 3$ for each structure. Simulations run for 50,000 timesteps.

then gray before repeating the cycle (Figure 6C). Testing the circuit with a higher blue ligand repression difficulty $\beta_{\text{BLUE-L}} = 11,000$ built a morphological oscillator that skipped the gray and blue phases, yielding a cyan red oscillator (Figure 6D). Oscillators with the remaining parameters ($\beta_{\text{BLUE-L}} = 16,000, 21,000$) are given in Figure S10. All these oscillations were highly reproducible and consistent ($n = 3$ each). $\beta_{\text{BLUE-L}} = 1000$ was a notably poor oscillator (Figure S10C). With the same parameters, the direct inhibition circuit and 2-TF permanent inhibition circuit did not yield oscillatory structures, confirming that temporary gene repression is the driver of oscillation (Figure S11).^{6,35,47–51}

Additional Temporal Control via Activating Amplifiers Improves Oscillation Quality. In addition to being able to build multicellular structures, inhibitory circuits can also generate morphological oscillations, demonstrating their potential for bottom-up synthetic development. It would be even more powerful, however, if the oscillations could be further modified and improved. The morphological oscillations generated by the temporary inhibition circuit damped quickly

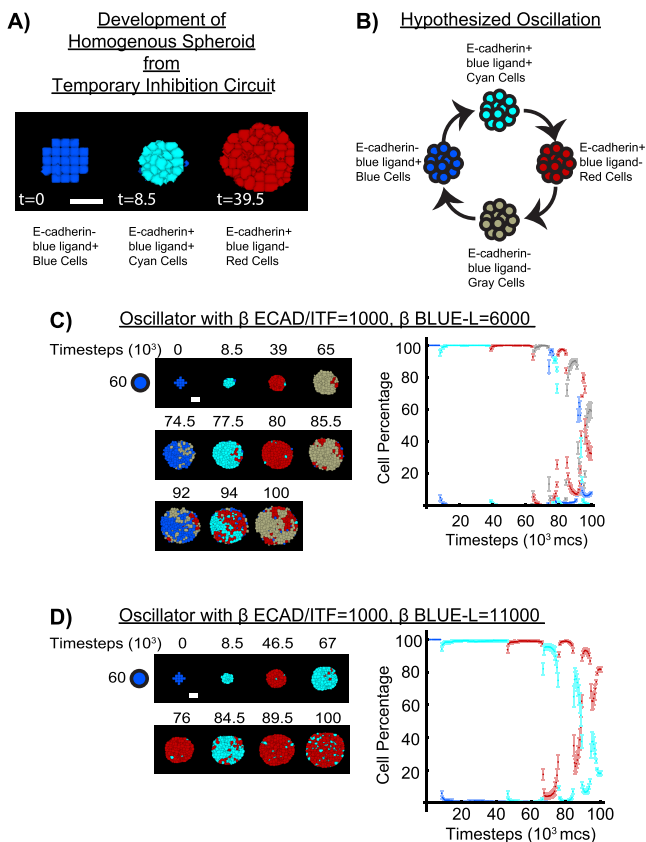


Figure 6. Temporary inhibition circuit can build oscillatory structures. (A) Homogenous spheroids built by the temporary inhibition circuit had cells synchronized in expression state (color) with sharp transition to the next expression state. An example developmental trajectory with these synchronous and sharp transitions is shown. Cell expression state is given below each image. (B) This led to the hypothesis that the temporary inhibition circuit can build oscillatory structures. Hypothesized oscillation is shown along with cell expression state for each phase in the oscillation. (C) 57 blue cells programmed with the temporary inhibition circuit and ECAD/ITF expression difficulty = 1000 (β ECAD/ITF = 1000) with blue ligand repression difficulty = 6000 (β BLUE-L = 6000) generated morphological oscillation. Cells synchronously transitioned from blue to cyan to red to gray before repeating the oscillation. Developmental trajectory shown is of images at the transition time. Plot of cell percentage is given as well. (D) 57 blue cells programmed with the temporary inhibition circuit but β ECAD/ITF = 1000 and β BLUE-L = 11,000. Oscillation differed from that of C, skipping the blue and gray phase. Developmental trajectory is shown along with plot of cell percentage. Additional oscillations with different parameters are given in Figure S10. A representative developmental trajectory is given per oscillation. $N = 3$ for each oscillation. Simulations run for 100,000 timesteps.

(Figure 6C,D). These results were confirmed by running the simulations for longer (Figure S12A,C).

In the accompanying study,¹⁸ activating transcriptional amplifiers were demonstrated to be capable of enacting spatiotemporal control over gene expression in bottom-up multicellular development. As temporary gene repression is what drives oscillation, using an activating amplifier to control the temporary gene repression of the temporary inhibition circuit could be a strategy to improve oscillation (Figure 7A). The circuit design (Figure 7B) is a simple modification of the temporary inhibition circuit; it uses an activating amplifier to control the inhibitory circuit of Figure 4C. The synNotch receptor now drives an activating amplifier consisting of an ATF

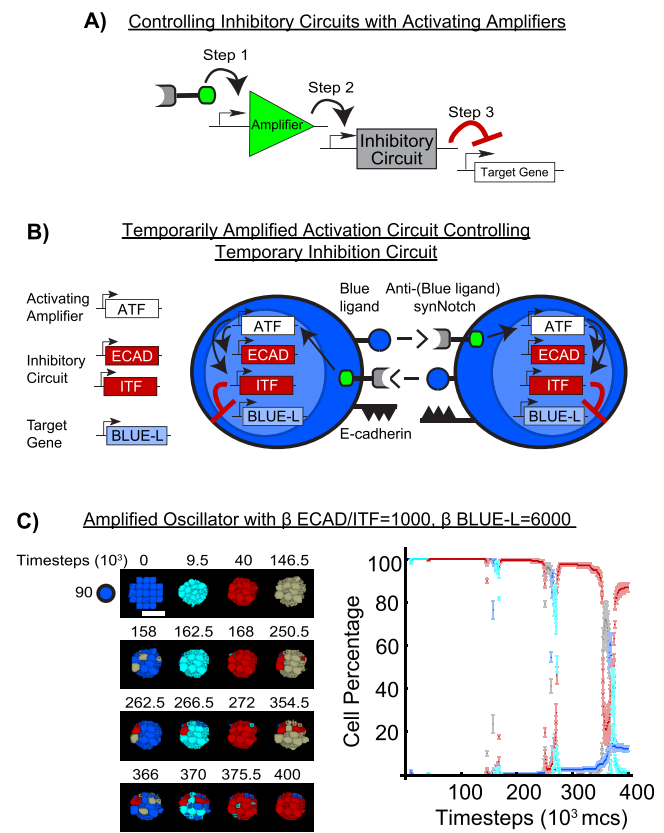


Figure 7. Using activating amplifiers to control the temporary inhibition circuit can improve oscillation quality. (A) The accompanying study describes how activating amplifiers can modulate temporal dynamics in synthetic circuits.¹⁸ Thus, prolonging repression with an activating amplifier could be a strategy to improve oscillation quality. (B) Temporarily amplified activation circuit controlling temporary inhibition circuit. The temporary inhibition circuit is rewired such that the synNotch receptor now drives the activating amplifier (activating transcription factor, ATF). The activating amplifier then drives the inhibitory circuit that then represses target gene expression. (C) Mixing 93 blue cells programmed with this circuit builds an oscillator with improved oscillation quality compared to its nonamplified variant (Figure S12A). Mitosis was removed due to computational limitations, but this does not affect timing or quality of oscillation (compare Figure 6C to Figure S12A, Figure 6D to Figure S12C). Developmental trajectory is shown along with plot of cell percentage. Additional oscillations with different parameters are given in Figures S12–14. A representative developmental trajectory is given per oscillation. $N = 3$ for each oscillation. Simulations run for 400,000 timesteps.

(Figure 7B). The ATF then drives expression of E-cadherin and ITF (Figure 7B). ITF then inhibits blue ligand expression as in the original circuit (Figure 7B).

Using the same parameters as the temporary inhibition circuit oscillator of Figure 6C and Figure S12A, the amplified oscillator improved morphological oscillation (Figure 7C). Oscillation quality between circuits was compared using the number of cyan phases completed before half amplitude (ring-down method in signal analysis).⁵² The cyan phase was chosen for quantification as it is present in all oscillators (i.e., cyan red oscillators lack gray and blue phases, Figure 6D) and does not have constant drift (i.e., see Figure S14B). Compared to its nonamplified variant (Figure 6C and Figure S12A), the amplified oscillator (Figure 7C) was approximately a 1.5-fold improvement in oscillation quality (3 cyan phases to 2 cyan phases). Due to prolonged inhibition from the activating amplifier,¹⁸ oscillations took

notably longer, requiring almost 400,000 timesteps for the three cycles (Figure 7C). Dampening was also observed but is notably less prominent. The oscillator of Figure S12A had red cell percentage quickly drift up with each red phase (5 to 20 to 50%) (Figure S12A). In contrast, the amplified oscillator had a much lower drift (0 to 5 to 20%) (Figure 7C).

Similar results were obtained for the β ECAD/ITF = 1000 β BLUE-L = 11,000 amplified oscillator (Figure S12B). The amplified oscillator was at least a 1.3-fold improvement in oscillation quality compared to its nonamplified counterpart (Figure S12C) (4 cyan phases to 3 cyan phases). The oscillation occurred over a longer duration due to prolonged inhibition from the activating amplifier as expected (Figure S12B). Dampening was observed but the amplified oscillator only had red percentage drift from 5 to 10 to 20% in the observed red phases (Figure S12B) while in the equivalent red phases of the oscillator, drift was from 0 to 40 to 70% (Figure S12C).

To confirm that oscillations are not limited to β ECAD/ITF = 1000 circuits, β ECAD/ITF = 6000 circuits were also tested for the capability to generate oscillatory structures. Oscillators with β ECAD/ITF = 6000 and β BLUE-L = 1000 or 6000 generated no oscillations (Figures S13A and 14A). However, the amplified oscillator circuits were able to oscillate (Figures S13B and 14B). These results indicate that incorporating activating amplifiers can not only improve but even rescue oscillations.

These results, in conjunction with those of Figure 6 and Figure S10, indicate that inhibitory circuits are powerful tools for achieving morphological oscillations. These circuits can be flexibly modified with additional circuits to alter their oscillatory behavior, supporting their utility for bottom-up synthetic development.

DISCUSSION

The bottom-up approach is an emerging but powerful strategy for studying multicellular development. Most bottom-up efforts focus on activatory circuits to drive synthetic development, but the results of this study predict that inhibitory circuits can also be powerful tools for driving development. The in silico approach recapitulates both native and synthetic inhibitory patterning, expected based on the original validation study,¹⁹ but more importantly, predicts that the designed inhibitory circuits are capable of building a variety of patterned multicellular structures. A systematic parameter scan reveals that the only known inhibitory structure to date is but a fraction of the structures possible. Further examination of one circuit revealed that it is capable of morphological oscillations and that these oscillations could be improved by using activatory circuits from the accompanying study. Altogether, these results support that inhibitory circuits can be powerful tools for building and studying developmental processes.

To demonstrate how inhibitory circuits can be used to build multicellular structures, a previously tested computational approach was deployed.^{18,19,36} The GSJM was combined with a cellular Potts framework to test the circuits across a variety of parameter combinations and show the numerous different morphologies buildable from these circuits (Figures 4 and 5, Figures S8–9).^{18,19,34} This computational setup has been validated for modeling and predicting the self-organizing structures that arise from synNotch-based circuits that drive differential adhesion,¹⁹ but it is always ideal to benchmark a computational approach against known systems from different contexts. Thus, the computational approach was benchmarked against a native system and was able to recapitulate the classic

“salt-and-pepper” patterning and even cell size bias in chicken hair cell development (Figure 3B and Figure S2).^{4,40} Against a synthetic system, the computational approach was able to recapitulate patterning resulting from both failed and successful repression (Figure 3C and Figure S7).⁴¹

The validation method of this study highlights another method to identify the optimal parameters for achieving a target pattern/structure. In the original study,¹⁹ the circuits were first parametrized to a test set of structures. The parametrized model was then used to predict the remaining structures. Here, as there is minimal starting information, the circuits were instead examined with a broad parameter scan to test if the circuits could recapitulate/predict known patterns and if so, identify the parameters optimal for them. When possible, the identified parameters can then be checked against remaining known patterns/structures for additional validation (as in Figure S8B). Thus, the optimal parameters for a target pattern/structure can be identified by two ways. Where there is sufficient starting information (i.e., several patterns and structures) to fit to, the model can be directly parametrized.¹⁹ Where there is minimal starting information (as here), then a broad parameter scan can be used instead to identify relevant parameters. Identified parameters can be checked against other known patterns/structures as quality assurance.

Either method can be used to identify the parameters, but there is a trade-off between the two. Compared to the direct parametrization method, the parameter scan method requires much more computational power and time as more simulations are needed. However, the parameter scan method is advantageous as it allows determining the extreme behavior of the circuits. This can provide valuable insight for circuit reengineering if the target behavior is not achieved. For example, circuits with poor repression (as in, Figure 3C top left) are a common obstacle in circuit engineering. In the temporary inhibition circuit, (and thus also the lateral inhibition circuit), this is often due to poor ITF induction. The typical biological remedy is to select for and use only cells transduced with high inducible ITF expression.^{10,41} Then, the in silico remedy is to decrease ITF expression difficulty by using a lower β ITF value.

The opposite, unwanted background activity, is also a common challenge in circuit engineering. For example, specific variants of the synNotch receptor can have high ligand-independent activity, leading to signaling independent repression.^{10,53,54} The biological fix is to either reengineer key regulatory domains of the receptor (i.e., transmembrane domain, juxtamembrane domain⁵⁴) or use another synNotch variant with low ligand-independent activity. In silico, the latter strategy is deployed; the model assumes the use of a low ligand-independent activity synNotch variant. Signal parameter S , modeling transcription factor (TF) released as a result of juxtacline ligand–receptor binding, only has value in the presence of juxtacline cognate ligand (receptor is assumed in excess as in^{18,19}). This model of the low background activity synNotch is used throughout the study, assuming a low ligand-independent activity synNotch variant is used biologically.

Independent of the obstacle, once the circuit is reengineered, the final check is to perform quality assurance. The whole circuit must have low background activity but have activity if the cognate ligand is present. Biologically, this is tested with coculture assays where circuit-imbedded cells are cultured with and without sender cells that bear the cognate ligand.^{10,31,32,54} The in silico check is analogous; circuit-imbedded cells are tested with (Figure 2) and without (Figure S1A) sender cells. The

results of **Figure 2** confirm that cells have activity if the cognate ligand is present. The results of **Figure S1A** validate that for repression difficulties ≥ 1000 , there is no background repression. In the accompanying study,¹⁸ I validated that expression difficulties ≥ 1000 do not have background expression. Thus, these two parameters must be ≥ 1000 to ensure background activity does not affect the results. Excluding the quality assurance check of **Figure S1A**, all other simulations fit these criteria (**Supplementary Table 1**). Overall, the *in silico* approach uses the same engineering and design logic as is used in the biological approach.

Another feature of the computational approach is that it models the receptor generically, rather than an exact receptor variant (i.e., anti-CD19 synNotch). This allows the computational approach to model a variety of synNotch circuits and expands its utility. In fact, because the approach calculates signal parameter S as juxtracrine ligand–receptor binding yielding TF release, the approach should be able to model other juxtracrine, TF-based receptors. This is demonstrated in the benchmark experiments of **Figure 3**. These systems did not use synNotch, but rather a native⁴⁰ or an enhanced Notch receptor.⁴¹ Thus, the computational approach can generically model juxtracrine, TF-based receptors, and is not limited to solely synNotch.¹⁸ This is fully expected as the GJSM component of the computational approach is mathematically equivalent to the Hill model,^{18,55,56} which historically has been used with success in modeling inhibitory signaling.^{3,4,35,46}

This generalized receptor modeling is powerful, but nonetheless has its limitations; the generalization limits the mechanistic features modelable. For instance, the *in vitro* patterning of **Figure 3C** top right was obtained by modifying the lateral inhibition circuit with increased basal Notch expression (through adding an exogenous Notch gene), increased Notch affinity and activity (though adding a glycosyltransferase that modifies Notch and acts as a positive feedback loop), and increased repressor induction (through selecting for high inducible ITF expression).⁴¹ In the computational approach, the increased basal receptor level can be directly modeled (see¹⁹ for the fully generalized version of the model) and increased repressor induction is modeled by lowering β ITF (as in **Figure 3C**). However, the current approach cannot model the glycosyltransferase mechanism, as signal parameter S is simply ligand–receptor binding equals TF release. An improved version of the model could have S as a function of the numerous processes that affect ligand–receptor binding and TF release (i.e., binding affinity, glycosylation status, cis-inhibition, cis-activation, efficiency of TF release by receptor, etc.).

An additional limitation is that the model cannot directly capture trafficking delay, and this is most notable in the direct inhibition circuit (**Figure S1C**). The direct inhibition circuit yields an immediate decrease in reporter level when exposed to sender cells (**Figure S1C**). Surprisingly, however, these fast dynamics are similar to what is observed *in vitro*, possibly because trafficking is fast compared to other circuit processes (i.e., ITF transcription/translation/production).^{31,32} Nonetheless, an improved version of the model should be able to directly model trafficking delay, as it is likely that different TFs have different trafficking times. It would be interesting to implement these circuits with slow trafficking TFs, as this could be another strategy to add temporal regulation.¹⁸ Future versions of the approach could use a time-delayed differential equation to model this.

Other avenues for improvement include adding support for cell extensions such as filopodia, as they have been reported to influence lateral inhibition patterning.⁵⁷ As this is a physical cell feature, it would have to be implemented into the *in silico* cells. It would be interesting to see how extensions affect, and if possible, could be controlled for, patterning synthetic structures since this has yet to be investigated. Another potential improvement is to include modeling for soluble ligands, which can yield intriguing “stellate like” patterns when combined with inhibitory signaling.⁵⁸

Some of the structures built by the inhibitory circuits are similar to those built by the activatory circuits of previous studies. For instance, the 2-layered structures of **Figure 4E** (structure 7), **Figure 5A** (structure 6), and **Figure 5B** (structure 5) are similar to the 2-layered structures built by the activatory circuits in refs 10 and 19. In contrast, the oscillatory structures of **Figures 6** and **7** may be examples of structures not achievable using activatory circuits. They require starting from a uniform cell population and cycling back to the initial uniform cell population. A purely activatory circuit, starting from a uniform cell population, is not expected to cycle back to the initial state as cells should activate without a means to synchronously revert.^{18,59} Future works incorporating the circuits designed here could provide valuable insight into what patterns/structures rely on inhibitory signaling, in line with the “build-it-to-understand-it” ideology.

It would be exciting to see what patterns/structures rely on inhibitory signaling, as this could provide hints as to what native developmental processes rely on inhibitory circuitry. As an example, the temporary inhibition circuit can generate cell synchronicity similar to that observed in somitogenesis, a native developmental process in which presomitic mesoderm cells synchronously segment to form multicellular somites.^{5,6,35,47,48,60,61} This suggests that a temporary repression mechanism could be mediating the oscillations of somitogenesis. Indeed, this has been previously proposed, simulated *in silico*,^{6,35,48} and supported experimentally.^{5,47,60,61} However, the exact inhibitory circuit for somitogenesis remains unknown. The temporary inhibition circuit is a candidate, but its rapid dampening suggests its oscillations are insufficient for sustaining somitogenesis (**Figure 6**). It is more likely that the temporary inhibition circuit is controlled by several other circuits that improve its stability. Then, the temporary inhibition circuit, when controlled by an activating amplifier, is a more likely candidate for somitogenesis. It oscillates for more cycles with less dampening (**Figure 7**). Realistically, the biological circuit(s) are likely to be far more complex as numerous other components have been implicated.^{5,6,35,48,60,61} Nonetheless, these results hint that these components could play an overall role of an activating amplifier for the temporary repression mechanism in order to generate stable oscillation.

As in the accompanying study,¹⁸ I designed the circuits generically to accommodate the rapidly increasing toolkit of synthetic biology.^{31,39,53,54,62–75} I leave the component choice to the user so that future components can be incorporated and tested. For example, typical TFs at the time of the lateral inhibition circuit included the ATFs Gal4-VP64, LexA-VP64, tTa, and ITF Gal4-KRAB.^{31,32,39,76–78} Since then, however, new TFs have emerged with improved compatibility and modularity.^{62–64,79}

These TF development efforts, like most bottom-up efforts, notably focus on gene activation. For bottom-up approaches to advance, there needs to be efforts toward developing new and

improved ITFs as well. As an example, the direct inhibition circuit that builds multicellular structures (Figure 5A) requires a bifunctional TF that can both inhibit and activate gene expression. Such a TF has yet to be engineered and used for multicellular synthetic development, but natural bifunctional TFs do exist and could be a viable starting point for this component.^{80–83}

Though the circuits here are relatively basic in design, they can build a wealth of patterned multicellular structures and even morphological oscillations. They even have features of native developmental processes such as cell fate divergence/bifurcation, self-organization, and synchronized oscillation. “Build-it-to-understand-it” efforts with inhibitory circuits could advance our understanding of native multicellular developmental processes. Beyond multicellular development, inhibitory circuits, like activatory circuits, could potentially be used for therapeutic purposes as well such as regenerative medicine and synthetic organ development.^{18,21,23,24} This work supports future research on inhibitory circuits, and I hope it will promote the use of inhibitory circuits in multicellular synthetic biology.

METHODS

Key Resources. Key resources are listed in Table 1.

Table 1. Key Resources

software or algorithm	source	identifier
CompuCell3D (CC3D) v3.7.8	ref 34	RRID:SCR_003052
Mathematica v12.0.0.0	Wolfram Research	RRID:SCR_014448
Excel v2310	Microsoft	RRID:SCR_016137
generalized juxtacline signaling model (GJSM)	ref 19	N/A
activating transcriptional amplifiers in GJSM	ref 18	N/A
ImageJ v1.54g	ref 84	RRID:SCR_003070

Lead Contact. Requests for information and code should be directed to Calvin Lam (calvin.lam.k@gmail). Example codes for the simulations of this study can be found at <https://github.com/calvinlamk/Inhibitory-Circuits-for-SynDev>.

In Silico Cell Line ISL929. ISL929 is an in silico cell line developed in ref 19 to model the in vitro L929 cell line used for building multicellular structures with the synNotch receptor.¹⁰ This line was developed in the CompuCell3D cellular Potts framework³⁴ and has been used with the GJSM to successfully predict how synNotch circuits can drive multicellular development.¹⁹ Because the synthetic Notch lateral inhibition circuit was implemented in L929 cells,¹⁰ ISL929 served as the ideal in silico cells for this study. It would allow checking the previous study’s results¹⁹ while also providing a biological experiment start point such as testing the inhibitory circuits from this study in L929 cells. A brief description of ISL929 is given in the accompanying study¹⁸ and a complete description is in the original study.¹⁹

Overview of the GJSM. The GJSM was developed to model synthetic juxtacline receptor (i.e., synNotch,^{10,31} SNIPR⁵⁴) regulation of gene expression.¹⁹ When parametrized, the model can capture synthetic juxtacline receptor signaling dynamics and has successfully predicted the developmental structures that arise from synNotch-based differential adhesion circuits.¹⁹ A brief description of the relevant model features is given below. Full descriptions can be found in refs 18 and 19.

Gene expression by a synthetic juxtacline receptor such as synNotch can be described by the general equation:

$$\frac{dR}{dt} = \frac{1}{1 + \exp[-(S - \beta)]} - \frac{R}{\kappa}$$

The change in the expressed gene’s protein level R at a given time step t is a function of both production (first term) and degradation (second term). In the production term, signal S models receptor or ATF signaling driving gene expression. β models gene expression difficulty and encompasses the biological processes that affect gene to functional protein product such as promoter, transcription, translation, expression delay, etc.^{18,19}

Degradation (second term) is modeled by the standard linear decay model. Protein product level R decays proportional to itself and inverse to decay constant κ . As a result, κ controls not only decay rate but saturation level as well.

The logistic form was chosen for GJSM over the Hill form for several reasons as described in the original study¹⁹ and accompanying study.¹⁸ First, the logistic form has simple and intuitive parameter interpretations that allow a user new to modeling to easily start. Weighing S against β allows a user to quickly understand how expression difficulty and signal affects expression. If S largely exceeds expression difficulty, then the expression is easy. If expression difficulty largely exceeds S , then the expression is difficult. Second, because the logistic form is mathematically equivalent to the Hill form, a more advanced user can convert the logistic equations to Hill equations to obtain more biologically relevant parameters if desired.^{18,55,56}

Because the logistic function is equivalent to the Hill function, GJSM is also capable of modeling gene repression. This was shown in the original study.¹⁹ Gene repression in GJSM can be described by the equation:

$$\frac{dR}{dt} = \frac{1}{1 + \exp[(S - \beta)]} - \frac{R}{\kappa}$$

This form is mathematically obtained by transforming the expression equation with S to $-S$ and β to $-\beta$.¹⁹ Signal S now models receptor or ITF signaling inhibiting gene expression. β now models gene repression difficulty and still encompasses the processes of the gene to functional protein product as in the expression equation. Intuitive interpretations remain and degradation modeling remains the same as in the expression equation.

Inhibitory Circuits as Modeled by GJSM. With the general equations described, equation sets for the inhibitory circuits can now be defined.

Direct Inhibition Circuit. In the direct inhibition circuit, the synNotch receptor directly inhibits target gene expression (Figure 1D). Then, the circuit equation is

$$\frac{dR}{dt} = \frac{1}{1 + \exp[(S_{SJR} - \beta_1)]} - \frac{R}{\kappa_1}$$

where S_{SJR} is the number of activated synNotch receptors at a given time step, with activated meaning bound to cognate ligand and released its TF. Parameters are as described above for inhibitory circuits. How S_{SJR} is calculated is shown below.

In the direct inhibition circuit for building multicellular structures (Figure 5A), the synNotch receptor also drives expression of the adhesion protein E-cadherin. E-cadherin levels are described by

$$\frac{dE_{cad}}{dt} = \frac{1}{1 + \exp[-(S_{SJR} - \beta_2)]} - \frac{E_{cad}}{\kappa_2}$$

S_{SJR} is the number of activated synNotch receptors at a given time step. Parameters are as described above for activatory circuits. How S_{SJR} is calculated is in a below section.

Temporary Inhibition Circuit/Oscillator Circuit. In the temporary inhibition circuit/oscillator circuit, the synNotch receptor indirectly inhibits gene expression by driving expression of an ITF that then inhibits target gene expression (Figure 1E). ITF levels are described by

$$\frac{d(ITE)}{dt} = \frac{1}{1 + \exp[-(S_{ITE} - \beta_1)]} - \frac{ITE}{\kappa_1}$$

Parameters are as described above for activatory circuits. Target gene product level R is then described by the inhibitory equation:

$$\frac{dR}{dt} = \frac{1}{1 + \exp[(S_{ITE} - \beta_2)]} - \frac{R}{\kappa_2}$$

S_{ITE} is the ITF level at a given time step from solving the first equation in the circuit. Parameters are as described above for inhibitory circuits.

In the temporary inhibition circuit for building multicellular structures (Figure 4) or oscillators (Figure 6), the synNotch receptor, in addition to driving the ITF, also drives the expression of E-cadherin. To simplify the number of parameters and equations used per circuit, E-cadherin levels are described by the ITF equation:

$$\frac{dE_{cad}}{dt} = \frac{1}{1 + \exp[-(S_{SJR} - \beta_1)]} - \frac{E_{cad}}{\kappa_1}$$

However, if desired, E-cadherin can be defined separately from ITF with its own parameters governing expression difficulty and decay.

2-TF Permanent Inhibition Circuit. In the 2-TF permanent inhibition circuit, the synNotch receptor drives the expression of the ATF and ITF (Figure 1F). The ATF is also able to drive the expression of the ATF and ITF (Figure 1F). Then, ATF levels are described by

$$\frac{d(ATF)}{dt} = \frac{1}{1 + \exp[-((S_{SJR} + S_{ATF}) - \beta_1)]} - \frac{ATF}{\kappa_1}$$

S_{ATF} is the ATF level from solving this equation at a given time step. Parameters are as described above for activatory circuits.

To simplify parameters and equations used and because the ITF is linked to ATF expression, the ITF is assigned the same equation:

$$\frac{d(ITE)}{dt} = \frac{1}{1 + \exp[-((S_{SJR} + S_{ATF}) - \beta_1)]} - \frac{ITE}{\kappa_1}$$

The ITF then inhibits target gene expression as in the temporary inhibition circuit. Thus, the equation is

$$\frac{dR}{dt} = \frac{1}{1 + \exp[(S_{ITE} - \beta_2)]} - \frac{R}{\kappa_2}$$

In the 2-TF permanent inhibition circuit for building multicellular structures (Figure 5B), in order to avoid the use of hybrid combinatorial promoters, which are not tested with GJSM,¹⁸ E-cadherin must be controlled by the same type of

promoter as the ATF/ITF. Because ATF is able to drive expression of itself through this promoter, E-cadherin must also be driven by the ATF. E-cadherin is also driven by the synNotch receptor. Then, to simplify the number of parameters and equations used per circuit, E-cadherin levels are described by the ATF/ITF equation:

$$\frac{dE_{cad}}{dt} = \frac{1}{1 + \exp[-((S_{SJR} + S_{ATF}) - \beta_1)]} - \frac{E_{cad}}{\kappa_1}$$

As in the temporary inhibition circuit, E-cadherin can be defined separately from ATF/ITF with its own parameters if desired.

Amplified Oscillator Circuit (Temporarily Amplified Activation Circuit Controlling Temporary Inhibition Circuit). In the amplified oscillator circuit, a temporarily amplified activation circuit controls the temporary inhibition circuit (Figure 7B). The synNotch receptor drives the expression of an ATF that then controls the temporary inhibition circuit.

The ATF equation is as in the published accompanying study:¹⁸

$$\frac{d(ATF)}{dt} = \frac{1}{1 + \exp[-(S_{SJR} - \beta_1)]} - \frac{ATF}{\kappa_1}$$

This ATF then drives expression of ITF and E-cadherin, replacing the role of the synNotch receptor in the temporary inhibition circuit. Then, the equations are

$$\begin{aligned}\frac{d(ITE)}{dt} &= \frac{1}{1 + \exp[-(S_{ATF} - \beta_2)]} - \frac{ITE}{\kappa_2} \\ \frac{dE_{cad}}{dt} &= \frac{1}{1 + \exp[-(S_{ATF} - \beta_2)]} - \frac{E_{cad}}{\kappa_2}\end{aligned}$$

Finally, the ITF then inhibits target gene expression as in the temporary inhibition circuit. Thus, the equation is

$$\frac{dR}{dt} = \frac{1}{1 + \exp[(S_{ITE} - \beta_3)]} - \frac{R}{\kappa_3}$$

For the equations of each circuit, parameters that do not change between equations are denoted with the same variable (i.e., β_1 is the same across all equations in the same circuit). However, it is important to note that parameters can be set differently between equations if desired. This confers additional flexibility in modeling but increases the parameters used for a circuit. Parameters are given in Supplementary Table 1.

Programming ISL929 Cells with Circuits and Receptors. Having defined the equations for each circuit, they were then implemented into ISL929 cells. See Figure S1A of the accompanying study for a graphical depiction of this process.¹⁸ The appropriate constitutive ligands were also added into the appropriate cells (i.e., orange ligands on orange cells). SynNotch was also added to the appropriate cells as well. To simplify calculations, synNotch was assumed to be in excess and nonlimiting as in the reference and accompanying studies.^{10,18,19} If desired, the complete GJSM framework can be used to model receptor-limiting cases. See the original study¹⁹ for the receptor-limiting formulation of GJSM. With these rules defined, it is now possible to calculate the signal S_{SJR} from synNotch signaling in the circuit equations. The relevant calculations are given here. The complete description and generalized formula can be found in the original study.¹⁹

SynNotch functions in a 1:1 stoichiometry; one activated receptor releases one TF regulating the target gene.^{18,19,31,32,54} Because synNotch is assumed to be in excess, S_{SJR} can be calculated from the amount of cognate ligand a focal cell is exposed to at the given time step. Then, S_{SJR} for a focal cell σ can be calculated using the following equation:

$$S_{\text{SJR}} = \sum_{\text{SN}} A_{\sigma-\text{SN}} \cdot \frac{L}{A_{\text{SN}}}$$

where $A_{\sigma-\text{SN}}$ is the surface area of σ contacting a particular signaling neighbor (SN), L is the amount of the cognate ligand on the SN surface, and A_{SN} is the SN's surface area. This formula is from the original GJSM study.¹⁹ For a focal cell σ , it receives SJR signal S_{SJR} calculated from the total number of cognate ligands it is exposed to at a given time step. For each signaling neighbor with the cognate ligand, dividing L by A_{SN} yields the ligand density. Multiplying this density by the shared surface area between the focal cell and SN gives the amount of ligand the focal cell sees from that single SN. Summing over all SNs then gives the total number of cognate ligands the focal cell is exposed to at a given time step and yields S_{SJR} .

L is a constant value for a constitutive ligand like an orange ligand, but for a ligand that is inhibited by the signaling circuit (i.e., blue ligand), L is defined by R in the circuit equations. Parameters are given in [Supplementary Table 1](#).

Linking Expression and Repression to Behavior.

Expression and repression were linked to intended behavior using a discrete transition model as in the original and accompanying study.^{18,19} A cell with a protein product level exceeding the threshold (7000 for all simulations in this study) gained the feature of the protein product. For example, exceeding 7000 for the E-cadherin level allows the cell to be adhesive to other E-cadherin expressing cells. Falling under this threshold results in the cell losing the feature. For example, an E-cadherin level falling under 7000 reverts the cell to nonadhesive. See the protocol³⁶ for a coding example of how to create in silico cells and program them with circuits and behaviors.

General Simulation Conditions. Each cell was initialized as a $5 \times 5 \times 5$ pixel cube. Data were collected every 100 timesteps for analysis. Blue cells were initialized at blue reporter/ligand saturation level κ .

Cell–Cell Signaling Assays. Cells were initialized in a $100 \times 100 \times 100$ lattice. Seeding configuration is described in the results section and in the accompanying study.¹⁸ Simulations run for 100,000 timesteps. Parameters are given in [Supplementary Table 1](#).

Monolayer Validation Assays. Cells were initialized in a $100 \times 100 \times 5$ lattice. Approximately 400 blue cells were initialized to create a cell monolayer and simulations run for 50,000 timesteps. Cell growth and mitosis were removed to prevent overcrowding and preserve the monolayer setup. A representative overhead image of the monolayer pattern for each parameter set is shown. The scalebar is 17.5 pixels to $100 \mu\text{m}$. To calculate size bias, the total surface area of blue LH cells for each lattice was calculated and then normalized to the number of blue LH cells. This was then repeated for blue LL cells, but normalized to the number of blue LL cells. The average surface area of blue LH cells was then normalized to the surface area of blue LL cells to calculate the relative size. As each parameter set was run in triplicates, this gave three lattices and three measurements of relative size. By averaging over lattices instead

of individual cells, this strategy mitigates lattice bias. Parameters are given in [Supplementary Table 1](#).

Quantifying Size Bias In Vivo. To quantify size bias in vivo, the same strategy was deployed as was in silico. The perimeter of each individual cell in chicken basilar papilla images from ref 40 were analyzed using ImageJ.⁸⁴ The images analyzed are given in [Figure 3B](#) and [Figure S2](#). Each cell had its perimeter measured using a region of interest, then cells were categorized into either HCA high (LH) or HCA low (LL) as determined by the original study's staining. For each image (analogous to an in silico lattice), the total perimeter of HCA high cells was calculated and then normalized to the number of HCA high cells. This was repeated with HCA low cells, but normalized to the number of HCA low cells. The average perimeter of HCA high cells was then normalized to the average perimeter of HCA low cells to yield the relative size. By averaging over three images instead of individual cells, this strategy, as was done in silico, mitigates lattice bias.

Building Multicellular Structure Simulations. Cells were initialized in a $100 \times 100 \times 100$ lattice. Cells were seeded as a spherical blob at the center of the lattice with the seeded number of cells given per experiment. Simulations were run for the timesteps given per experiment. Representative cross sections of the structures are shown as in the reference *in vitro* experiment.¹⁰ The scalebar is 17.5 pixels to $100 \mu\text{m}$ as determined in the original study.¹⁹ Cell percentage was calculated by dividing the number of cells of the focal type over the total number of cells in the simulation at that time step. Parameters are given in [Supplementary Table 1](#).

Mitosis Removal. Cell growth and mitosis were removed in oscillation simulations with runtime $>100,000$ timesteps. The longer runtime required for observing oscillation along with its termination would otherwise result in cells completely filling the lattice and slowing the simulation significantly. It was validated that growth and mitosis removal did not affect oscillation (compare [Figure 6C](#) to [Figure S12A](#), [Figure 6D](#) to [Figure S12C](#)). Cells sharply transitioned at the same time points and transitioned to the correct phase independent of growth and mitosis.

Comparing Oscillation Quality. To roughly compare oscillation quality between circuits, the quality factor Q for each oscillation was calculated using the ring-down method.⁵² Q , the quality of the oscillation, can be defined proportionate to the number of oscillations before the oscillation decays to 50% of its maximum amplitude. 100% was used as the maximum amplitude and Q was calculated off the cyan phase of the oscillation as it is present in all oscillators and does not have constant drift. Q was then compared between circuits to calculate the fold improvement.

Statistical Analysis. t test was used to test for size differences between LH and LL cells. Sample size is given in the text, figures, or captions. Plots are mean \pm SEM.

ASSOCIATED CONTENT

SI Supporting Information

The Supporting Information is available free of charge at <https://pubs.acs.org/doi/10.1021/acssynbio.4c00230>.

Images and quantifications from testing the model against native and synthetic inhibitory processes; for the designed circuits, the full gallery of structures along with images of oscillation and quantification ([PDF](#))

Parameters used for all the simulations of these experiments ([XLSX](#))

AUTHOR INFORMATION

Corresponding Author

Calvin Lam — *Independent Investigator, Department of Biochemistry and Molecular Biology, University of Nebraska Medical Center, Omaha, Nebraska 68198, United States;*  [orcid.org/0000-0003-2768-4230](#); Email: calvin.lam.k@gmail.com

Complete contact information is available at:
<https://pubs.acs.org/10.1021/acssynbio.4c00230>

Author Contributions

C.L. conceived, designed, performed, analyzed, and wrote the entire study.

Funding

This work was not funded by any private or public agency. The author solely funded this study by himself through trading highly leveraged financial derivatives.

Notes

The author declares no competing financial interest.

ACKNOWLEDGMENTS

I would like to thank UNMC for access to and aid in printing research articles. I am thankful to the three anonymous reviewers of my previous article¹⁸ and the reviewers of this article as their suggestions have helped improve this manuscript.

REFERENCES

- (1) Cohen, R.; Taiber, S.; Loza, O.; Kasirer, S.; Woland, S.; Sprinzak, D. Precise Alternating Cellular Pattern in the Inner Ear by Coordinated Hopping Intercalations and Delaminations. *Sci. Adv.* **2023**, *9* (8), No. eadd2157.
- (2) Sprinzak, D.; Lakhampal, A.; LeBon, L.; Garcia-Ojalvo, J.; Elowitz, M. B. Mutual Inactivation of Notch Receptors and Ligands Facilitates Developmental Patterning. *PLoS Comput. Biol.* **2011**, *7* (6), No. e1002069.
- (3) Sprinzak, D.; Lakhampal, A.; LeBon, L.; Santat, L. A.; Fontes, M. E.; Anderson, G. A.; Garcia-Ojalvo, J.; Elowitz, M. B. Cis-Interactions between Notch and Delta Generate Mutually Exclusive Signalling States. *Nature* **2010**, *465* (7294), 86–90.
- (4) Shaya, O.; Binstok, U.; Hersch, M.; Rivkin, D.; Weinreb, S.; Amir-Zilberman, L.; Khamaisi, B.; Oppenheim, O.; Desai, R. A.; Goodyear, R. J.; Richardson, G. P.; Chen, C. S.; Sprinzak, D. Cell-Cell Contact Area Affects Notch Signaling and Notch-Dependent Patterning. *Dev. Cell* **2017**, *40* (5), 505.e6–511.e6.
- (5) Miao, Y.; Djeffal, Y.; De Simone, A.; Zhu, K.; Lee, J. G.; Lu, Z.; Silberfeld, A.; Rao, J.; Tarazona, O. A.; Mongera, A.; Rigoni, P.; Diaz-Cuadros, M.; Song, L. M. S.; Di Talia, S.; Pourquié, O. Reconstruction and Deconstruction of Human Somitogenesis in Vitro. *Nature* **2023**, *614*, 500.
- (6) Goldbeter, A.; Pourquié, O. Modeling the Segmentation Clock as a Network of Coupled Oscillations in the Notch, Wnt and FGF Signaling Pathways. *J. Theor. Biol.* **2008**, *252* (3), 574–585.
- (7) Palmer, M. A.; Nerger, B. A.; Goodwin, K.; Sudhakar, A.; Lemke, S. B.; Ravindran, P. T.; Toettcher, J. E.; Košmrlj, A.; Nelson, C. M. Stress Ball Morphogenesis: How the Lizard Builds Its Lung. *Sci. Adv.* **2023**, *7* (52), No. eabk0161.
- (8) Steinberg, M. S. Reconstruction of Tissues by Dissociated Cells. *Science* **1979**, *141* (3579), 401–408.
- (9) Foty, R. A.; Steinberg, M. S. The Differential Adhesion Hypothesis: A Direct Evaluation. *Dev. Biol.* **2005**, *278* (1), 255–263.
- (10) Toda, S.; Blauch, L. R.; Tang, S. K. Y.; Morsut, L.; Lim, W. A. Programming Self-Organizing Multicellular Structures with Synthetic Cell-Cell Signaling. *Science* **1979**, *361* (6398), 156–162.
- (11) Toda, S.; McKeithan, W. L.; Hakkinen, T. J.; Lopez, P.; Klein, O. D.; Lim, W. A. Engineering Synthetic Morphogen Systems That Can Program Multicellular Patterning. *Science* **1979**, *370* (6514), 327–331.
- (12) Lam, C.; Li, Y.; Landgraf, T.; Nieh, J. Dancing Attraction: Followers of Honey Bee Tremble and Waggle Dances Exhibit Similar Behaviors. *Biol. Open* **2017**, *6* (6), 810–817.
- (13) Schlissel, G.; Li, P. Synthetic Developmental Biology: Understanding Through Reconstitution. *Annu. Rev. Cell Dev. Biol.* **2020**, *36* (1), 339–357.
- (14) Li, P.; Markson, J. S.; Wang, S.; Chen, S.; Vachharajani, V.; Elowitz, M. B. Morphogen Gradient Reconstitution Reveals Hedgehog Pathway Design Principles. *Science* **1979**, *360* (6388), 543–548.
- (15) McNamara, H. M.; Ramm, B.; Toettcher, J. E. Synthetic Developmental Biology: New Tools to Deconstruct and Rebuild Developmental Systems. *Semin Cell Dev Biol.* **2023**, *141*, 33–42.
- (16) Ho, C.; Morsut, L. Novel Synthetic Biology Approaches for Developmental Systems. *Stem Cell Reports* **2021**, *16* (5), 1051–1064.
- (17) Toda, S.; Frankel, N. W.; Lim, W. A. Engineering Cell–Cell Communication Networks: Programming Multicellular Behaviors. *Curr. Opin Chem. Biol.* **2019**, *52*, 31–38.
- (18) Lam, C. Design and Mathematical Analysis of Activating Transcriptional Amplifiers That Enable Modular Temporal Control in Synthetic Juxtacrine Circuits. *Synth Syst. Biotechnol* **2023**, *8* (4), 654–672.
- (19) Lam, C.; Saluja, S.; Courcoubetis, G.; Yu, D.; Chung, C.; Courte, J.; Morsut, L. Parameterized Computational Framework for the Description and Design of Genetic Circuits of Morphogenesis Based on Contact-Dependent Signaling and Changes in Cell–Cell Adhesion. *ACS Synth. Biol.* **2022**, *11* (4), 1417–1439.
- (20) Santorelli, M.; Lam, C.; Morsut, L. Synthetic Development: Building Mammalian Multicellular Structures with Artificial Genetic Programs. *Curr. Opin Biotechnol* **2019**, *59*, 130–140.
- (21) Johnson, M. B.; March, A. R.; Morsut, L. Engineering Multicellular Systems: Using Synthetic Biology to Control Tissue Self-Organization. *Curr. Opin Biomed Eng.* **2017**, *4*, 163–173.
- (22) Mukherji, S.; van Oudenaarden, A. Synthetic Biology: Understanding Biological Design from Synthetic Circuits. *Nat. Rev. Genet* **2009**, *10* (12), 859–871.
- (23) Zarkesh, I.; Kazemi Ashtiani, M.; Shiri, Z.; Aran, S.; Braun, T.; Baharvand, H. Synthetic Developmental Biology: Engineering Approaches to Guide Multicellular Organization. *Stem Cell Reports* **2022**, *17* (4), 715–733.
- (24) Lee, J. C.; Walton, B. L.; Hamann, C. A.; Brunger, J. M. Synthetic Regulation of Multicellular Systems for Regenerative Engineering. *Curr. Opin Biomed Eng.* **2020**, *16*, 42–51.
- (25) Kim, H.; Jin, X.; Glass, D. S.; Riedel-Kruse, I. H. Engineering and Modeling of Multicellular Morphologies and Patterns. *Curr. Opin Genet Dev* **2020**, *63*, 95–102.
- (26) Lim, W. A. The Emerging Era of Cell Engineering: Harnessing the Modularity of Cells to Program Complex Biological Function. *Science (1979)* **2022**, *378* (6622), 848–852.
- (27) Martinez-Ara, G.; Staporwongkul, K. S.; Ebisuya, M. Scaling up Complexity in Synthetic Developmental Biology. *Science (1979)* **2022**, *378* (6622), 864–868.
- (28) Trentesaux, C.; Yamada, T.; Klein, O. D.; Lim, W. A. Harnessing Synthetic Biology to Engineer Organoids and Tissues. *Cell Stem Cell* **2023**, *30* (1), 10–19.
- (29) Elowitz, M.; Lim, W. A. Build Life to Understand It. *Nature* **2010**, *468* (7326), 889–890.
- (30) Zhu, R.; Santat, L. A.; Markson, J. S.; Nandagopal, N.; Gregowicz, J.; Elowitz, M. B. Reconstitution of Morphogen Shutting Circuits. *Sci. Adv.* **2023**, *9* (28), No. eadf9336.
- (31) Morsut, L.; Roybal, K. T.; Xiong, X.; Gordley, R. M.; Coyle, S. M.; Thomson, M.; Lim, W. A. Engineering Customized Cell Sensing and Response Behaviors Using Synthetic Notch Receptors. *Cell* **2016**, *164* (4), 780–791.

- (32) Roybal, K. T.; Rupp, L. J.; Morsut, L.; Walker, W. J.; McNally, K. A.; Park, J. S.; Lim, W. A. Precision Tumor Recognition by T Cells With Combinatorial Antigen-Sensing Circuits. *Cell* **2016**, *164* (4), 770–779.
- (33) Izaguirre, J. A.; Chaturvedi, R.; Huang, C.; Cickovski, T.; Coffland, J.; Thomas, G.; Forgacs, G.; Alber, M.; Hentschel, G.; Newman, S. A.; Glazier, J. A. CompuCell, a Multi-Model Framework for Simulation of Morphogenesis. *Bioinformatics* **2004**, *20* (7), 1129–1137.
- (34) Swat, M. H.; Thomas, G. L.; Belmonte, J. M.; Shirinifard, A.; Hmeljak, D.; Glazier, J. A. Chapter 13 - Multi-Scale Modeling of Tissues Using CompuCell3D. In *Methods in Cell Biology*; Asthagiri, A. R.; Arkin, A. P., Eds.; Academic Press, 2012; Vol. 110, pp 325–366.
- (35) Hester, S. D.; Belmonte, J. M.; Gens, J. S.; Clendenon, S. G.; Glazier, J. A. A Multi-Cell, Multi-Scale Model of Vertebrate Segmentation and Somite Formation. *PLoS Comput. Biol.* **2011**, *7* (10), No. e1002155.
- (36) Lam, C.; Morsut, L. Programming Juxtacrine-Based Synthetic Signaling Networks in a Cellular Potts Framework. In *Synthetic Biology: Methods and Protocols*; Braman, J. C., Ed.; Springer US: New York, NY, 2024; pp 283–307.
- (37) Burrill, D. R.; Inniss, M. C.; Boyle, P. M.; Silver, P. A. Synthetic Memory Circuits for Tracking Human Cell Fate. *Genes Dev.* **2012**, *26* (13), 1486–1497.
- (38) Ajo-Franklin, C. M.; Drubin, D. A.; Eskin, J. A.; Gee, E. P. S.; Landgraf, D.; Phillips, I.; Silver, P. A. Rational Design of Memory in Eukaryotic Cells. *Genes Dev.* **2007**, *21* (18), 2271–2276.
- (39) Zhou, J.; Ge, Q.; Wang, D.; Guo, Q.; Tao, Y. Engineering a Modular Double-Transmembrane Synthetic Receptor System for Customizing Cellular Programs. *Cell Rep.* **2023**, *42* (4), No. 112385.
- (40) Goodear, R.; Richardson, G. Pattern Formation in the Basilar Papilla: Evidence for Cell Rearrangement. *J. Neurosci.* **1997**, *17* (16), 6289.
- (41) Matsuda, M.; Koga, M.; Woltjen, K.; Nishida, E.; Ebisuya, M. Synthetic Lateral Inhibition Governs Cell-Type Bifurcation with Robust Ratios. *Nat. Commun.* **2015**, *6* (1), 6195.
- (42) Cohen, R.; Taiber, S.; Loza, O.; Kasirer, S.; Woland, S.; Sprinzak, D. Precise Alternating Cellular Pattern in the Inner Ear by Coordinated Hopping Intercalations and Delaminations. *Sci. Adv.* **2023**, *9* (8), No. eadd2157.
- (43) Hunter, G. L.; Hadjivassiliou, Z.; Bonin, H.; He, L.; Perrimon, N.; Charras, G.; Baum, B. Coordinated Control of Notch/Delta Signalling and Cell Cycle Progression Drives Lateral Inhibition-Mediated Tissue Patterning. *Development* **2016**, *143* (13), 2305–2310.
- (44) Liao, B.-K.; Oates, A. C. Delta-Notch Signalling in Segmentation. *Arthropod Struct Dev.* **2017**, *46* (3), 429–447.
- (45) Siebel, C.; Lendahl, U. Notch Signaling in Development, Tissue Homeostasis, and Disease. *Physiol Rev.* **2017**, *97* (4), 1235–1294.
- (46) Collier, J. R.; Monk, N. A. M.; Maini, P. K.; Lewis, J. H. Pattern Formation by Lateral Inhibition with Feedback: A Mathematical Model of Delta-Notch Intercellular Signalling. *J. Theor. Biol.* **1996**, *183* (4), 429–446.
- (47) Saga, Y. The Mechanism of Somite Formation in Mice. *Curr. Opin. Genet. Dev.* **2012**, *22* (4), 331–338.
- (48) Lewis, J. Autoinhibition with Transcriptional Delay: A Simple Mechanism for the Zebrafish Somitogenesis Oscillator. *Curr. Biol.* **2003**, *13* (16), 1398–1408.
- (49) Elowitz, M. B.; Leibler, S. A Synthetic Oscillatory Network of Transcriptional Regulators. *Nature* **2000**, *403* (6767), 335–338.
- (50) Santorelli, M.; Perna, D.; Isomura, A.; Garzilli, I.; Annunziata, F.; Postiglione, L.; Tumaini, B.; Kageyama, R.; di Bernardo, D. Reconstitution of an Ultradian Oscillator in Mammalian Cells by a Synthetic Biology Approach. *ACS Synth. Biol.* **2018**, *7* (5), 1447–1455.
- (51) Tigges, M.; Marquez-Lago, T. T.; Stelling, J.; Fussenegger, M. A Tunable Synthetic Mammalian Oscillator. *Nature* **2009**, *457* (7227), 309–312.
- (52) Startin, W. J.; Beilby, M. A.; Saulson, P. R. Mechanical Quality Factors of Fused Silica Resonators. *Rev. Sci. Instrum.* **1998**, *69* (10), 3681–3689.
- (53) Yang, Z.; Yu, Z.; Cai, Y.; Du, R.; Cai, L. Engineering of an Enhanced Synthetic Notch Receptor by Reducing Ligand-Independent Activation. *Commun. Biol.* **2020**, *3* (1), 116.
- (54) Zhu, I.; Liu, R.; Garcia, J. M.; Hyrenius-Wittsten, A.; Piraner, D. I.; Alavi, J.; Israni, D. V.; Liu, B.; Khalil, A. S.; Roybal, K. T. Modular Design of Synthetic Receptors for Programmed Gene Regulation in Cell Therapies. *Cell* **2022**, *185* (8), 1431.e16–1443.e16.
- (55) Reeve, R.; Turner, J. R. Pharmacodynamic Models: Parameterizing the Hill Equation, Michaelis-Menten, the Logistic Curve, and Relationships Among These Models. *J. Biopharm Stat.* **2013**, *23* (3), 648–661.
- (56) Barlow, R.; Blake, J. F. Hill Coefficients and the Logistic Equation. *Trends Pharmacol. Sci.* **1989**, *10* (11), 440–441.
- (57) Cohen, M.; Georgiou, M.; Stevenson, N. L.; Miodownik, M.; Baum, B. Dynamic Filopodia Transmit Intermittent Delta-Notch Signaling to Drive Pattern Refinement during Lateral Inhibition. *Dev. Cell* **2010**, *19* (1), 78–89.
- (58) Duran-Nebreda, S.; Pla, J.; Vidiella, B.; Piñero, J.; Conde-Pueyo, N.; Solé, R. Synthetic Lateral Inhibition in Periodic Pattern Forming Microbial Colonies. *ACS Synth. Biol.* **2021**, *10* (2), 277–285.
- (59) Santorelli, M.; Bhamidipati, P. S.; Kavanagh, A.; MacKrell, V. A.; Sondkar, T.; Thomson, M.; Morsut, L. Control of Spatio-Temporal Patterning via Cell Density in a Multicellular Synthetic Gene Circuit. *bioRxiv* **2022**, No. 2022.10.04.510900.
- (60) Cinquin, O. Understanding the Somitogenesis Clock: What's Missing? *Mech. Dev.* **2007**, *124* (7), S01–S17.
- (61) Miao, Y.; Pourquié, O. Cellular and Molecular Control of Vertebrate Somitogenesis. *Nat. Rev. Mol. Cell Biol.* **2024**, DOI: [10.1038/s41580-024-00709-z](https://doi.org/10.1038/s41580-024-00709-z).
- (62) Chen, W. C. W.; Gaidukov, L.; Lai, Y.; Wu, M.-R.; Cao, J.; Gutbrod, M. J.; Choi, G. C. G.; Utomo, R. P.; Chen, Y.-C.; Wroblewska, L.; Kellis, M.; Zhang, L.; Weiss, R.; Lu, T. K. A Synthetic Transcription Platform for Programmable Gene Expression in Mammalian Cells. *Nat. Commun.* **2022**, *13* (1), 6167.
- (63) Li, H.-S.; Israni, D. V.; Gagnon, K. A.; Gan, K. A.; Raymond, M. H.; Sander, J. D.; Roybal, K. T.; Joung, J. K.; Wong, W. W.; Khalil, A. S. Multidimensional Control of Therapeutic Human Cell Function with Synthetic Gene Circuits. *Science (1979)* **2022**, *378* (6625), 1227–1234.
- (64) Krawczyk, K.; Scheller, L.; Kim, H.; Fussenegger, M. Rewiring of Endogenous Signaling Pathways to Genomic Targets for Therapeutic Cell Reprogramming. *Nat. Commun.* **2020**, *11* (1), 608.
- (65) Liu, H.; Baeumler, T. A.; Nakamura, K.; Okada, Y.; Cho, S.; Eguchi, A.; Kuroda, D.; Tsumoto, K.; Ueki, R.; Sando, S. An Engineered Synthetic Receptor–Aptamer Pair for an Artificial Signal Transduction System. *ACS Nano* **2023**, *17* (10), 9039–9048.
- (66) Huang, J.; Xue, S.; Buchmann, P.; Teixeira, A. P.; Fussenegger, M. An Electrogenetic Interface to Program Mammalian Gene Expression by Direct Current. *Nat. Metab.* **2023**, *5* (8), 1395–1407.
- (67) Sloas, D. C.; Tran, J. C.; Marzilli, A. M.; Ngo, J. T. Tension-Tuned SynNotch Receptors for Synthetic Mechanotransduction and Intercellular Force Detection. *bioRxiv* **2022**, No. 2022.05.01.490205.
- (68) Conklin, B. R.; Hsiao, E. C.; Claeyse, S.; Dumuis, A.; Srinivasan, S.; Forsayeth, J. R.; Guettier, J.-M.; Chang, W. C.; Pei, Y.; McCarthy, K. D.; Nissensohn, R. A.; Wess, J.; Bockaert, J.; Roth, B. L. Engineering GPCR Signaling Pathways with RASSLs. *Nat. Methods* **2008**, *5* (8), 673–678.
- (69) Hartfield, R. M.; Schwarz, K. A.; Muldoon, J. J.; Bagheri, N.; Leonard, J. N. Multiplexing Engineered Receptors for Multiparametric Evaluation of Environmental Ligands. *ACS Synth. Biol.* **2017**, *6* (11), 2042–2055.
- (70) Edelstein, H. I.; Donahue, P. S.; Muldoon, J. J.; Kang, A. K.; Dolberg, T. B.; Battaglia, L. M.; Allchin, E. R.; Hong, M.; Leonard, J. N. Elucidation and Refinement of Synthetic Receptor Mechanisms. *Synth. Biol.* **2020**, *5* (1), No. ysaa017.
- (71) Schwarz, K. A.; Daringer, N. M.; Dolberg, T. B.; Leonard, J. N. Rewiring Human Cellular Input–Output Using Modular Extracellular Sensors. *Nat. Chem. Biol.* **2017**, *13* (2), 202–209.

- (72) Daringer, N. M.; Dudek, R. M.; Schwarz, K. A.; Leonard, J. N. Modular Extracellular Sensor Architecture for Engineering Mammalian Cell-Based Devices. *ACS Synth. Biol.* **2014**, *3* (12), 892–902.
- (73) Scheller, L.; Strittmatter, T.; Fuchs, D.; Bojar, D.; Fussenegger, M. Generalized Extracellular Molecule Sensor Platform for Programming Cellular Behavior. *Nat. Chem. Biol.* **2018**, *14* (7), 723–729.
- (74) Kipniss, N. H.; Dingal, P. C. D. P.; Abbott, T. R.; Gao, Y.; Wang, H.; Dominguez, A. A.; Labanieh, L.; Qi, L. S. Engineering Cell Sensing and Responses Using a GPCR-Coupled CRISPR-Cas System. *Nat. Commun.* **2017**, *8* (1), 2212.
- (75) Barnea, G.; Strapps, W.; Herrada, G.; Berman, Y.; Ong, J.; Kloss, B.; Axel, R.; Lee, K. J. The Genetic Design of Signaling Cascades to Record Receptor Activation. *Proc. Natl. Acad. Sci. U. S. A.* **2008**, *105* (1), 64–69.
- (76) Williams, J. Z.; Allen, G. M.; Shah, D.; Sterin, I. S.; Kim, K. H.; Garcia, V. P.; Shavey, G. E.; Yu, W.; Puig-Saus, C.; Tsui, J.; Ribas, A.; Roybal, K. T.; Lim, W. A. Precise T Cell Recognition Programs Designed by Transcriptionally Linking Multiple Receptors. *Science* (1979) **2020**, *370* (6520), 1099–1104.
- (77) Lam, C. K.; Hyde, R. K.; Patel, S. A. Synthetic Immunotherapy: Programming Immune Cells with Novel and Sophisticated Logic Capabilities. *Transplant Cell Ther.* **2022**, *28* (9), 560–571.
- (78) Roybal, K. T.; Williams, J. Z.; Morsut, L.; Rupp, L. J.; Kolinko, I.; Choe, J. H.; Walker, W. J.; McNally, K. A.; Lim, W. A. Engineering T Cells with Customized Therapeutic Response Programs Using Synthetic Notch Receptors. *Cell* **2016**, *167* (2), 419.e16–432.e16.
- (79) Baeumler, T. A.; Ahmed, A. A.; Fulga, T. A. Engineering Synthetic Signaling Pathways with Programmable DCas9-Based Chimeric Receptors. *Cell Rep* **2017**, *20* (11), 2639–2653.
- (80) Scully, K. M.; Jacobson, E. M.; Jepsen, K.; Lunyak, V.; Viadiu, H.; Carrière, C.; Rose, D. W.; Hooshmand, F.; Aggarwal, A. K.; Rosenfeld, M. G. Allosteric Effects of Pit-1 DNA Sites on Long-Term Repression in Cell Type Specification. *Science* (1979) **2000**, *290* (5494), 1127–1131.
- (81) Willy, P. J.; Kobayashi, R.; Kadonaga, J. T. A Basal Transcription Factor That Activates or Represses Transcription. *Science* (1979) **2000**, *290* (5493), 982–984.
- (82) Latchman, D. S. Transcription Factors: Bound to Activate or Repress. *Trends Biochem. Sci.* **2001**, *26* (4), 211–213.
- (83) Boyle, P.; Després, C. Dual-Function Transcription Factors and Their Entourage. *Plant Signal Behav.* **2010**, *5* (6), 629–634.
- (84) Schneider, C. A.; Rasband, W. S.; Eliceiri, K. W. NIH Image to ImageJ: 25 Years of Image Analysis. *Nat. Methods* **2012**, *9* (7), 671–675.



CAS BIOFINDER DISCOVERY PLATFORM™

PRECISION DATA FOR FASTER DRUG DISCOVERY

CAS BioFinder helps you identify targets, biomarkers, and pathways

Unlock insights

CAS 
A division of the
American Chemical Society